Compositional Radio Map Reconstruction for Wi-Fi RSS Localization With Partial Environmental-State Surveys

Chengjie HOU, Xianbo SUN, Yong HUANG, Qinghua ZHU, Jinqiao YI, Tao HU, Lin GAO, Li ZHU, Mian XIANG*

College of Intelligent Systems Science and Engineering, Hubei Minzu University, Enshi, China

*632263828@qq.com

Submitted June 3, 2026 / Accepted July 24, 2026 / Online first August 7, 2026

Abstract. *Wi-Fi received signal strength (RSS) fingerprint localization is sensitive to structural state changes because opening or closing doors and partitions changes propagation paths and may require state-specific radio maps. Existing state-aware multi-fingerprint localization can handle such changes only after the fingerprint database of each state has been surveyed, leading to 2^H surveys for H variable elements. This paper proposes CoStateLoc (Compositional State-Conditioned Localization), a survey-efficient framework that reconstructs unseen-state radio maps from baseline, single-factor, and selected dual-factor surveys. CoStateLoc represents each state-specific fingerprint database as a combination of a baseline map, single-factor perturbations, and sparse pairwise interactions estimated directly from surveyed databases. A controlled two-dimensional (2D) geometric ray-tracing simulator is used to evaluate the reconstruction mechanism. For H=6 doors (64 states) in three geometrically different layouts, CoStateLoc uses 22 surveyed states and reduces the survey count by 65.6%. Under the adopted simulation model and known-state assumption, it achieves up to 20.4% lower mean localization error than a first-order additive baseline and outperforms a Hamming-kernel state-generation baseline. The results provide controlled simulation evidence rather than deployment-level validation.*

Keywords

Indoor localization, Wi-Fi RSS fingerprinting, environmental state variation, radio map reconstruction, incomplete site survey, ray tracing

1. Introduction

With the rapid development of mobile Internet and smart devices, indoor location information has become an important basis for navigation, context-aware service, emergency management, and intelligent building applications. Global Navigation Satellite Systems can provide reliable positioning in outdoor scenes, but their signals are often blocked or strongly attenuated inside buildings [1], [2]. Among indoor positioning technologies, Wi-Fi received signal strength (RSS) fingerprint localization has attracted continuous attention because Wi-Fi access points (APs) are widely deployed and RSS measurements can be obtained without extra positioning hardware [3–6]. Beyond localization, radio-frequency (RF) sensing has also been used for indoor perception tasks such as millimeter-wave-radar human motion recognition and device-free sensing [7], [8].

A typical Wi-Fi fingerprint localization system contains an offline phase and an online phase. In the offline phase, RSS values from multiple APs are collected at known reference points (RPs) to construct a radio map. In the online phase, the RSS vector measured by the target user is compared with the stored fingerprints, and the position is estimated by matching algorithms such as k-nearest-neighbor (KNN), weighted KNN (WKNN), or probabilistic inference [5, 9–11]. This scheme is effective when the radio map used online has the same statistical characteristics as the environment in which it was collected. However, the RSS fingerprint is not determined only by the RP coordinate. It is also affected by reflection, penetration, diffraction, and line-of-sight conditions along the AP-RP propagation paths, and practical deployment studies have repeatedly reported that RSS fluctuation, AP reliability, AP changes, and site-survey cost limit the robustness of fingerprint systems [12–15].

In practical indoor environments, spatial structures are not always fixed. Doors, partitions, and movable walls may be opened, closed, or rearranged, which can change a propagation path from penetration-dominated transmission to reflection or line-of-sight transmission. A previous multi-fingerprint study showed that such environmental state changes may cause RSS shifts greater than 20 dB at the same position, so a single fingerprint database cannot accurately represent all spatial states [16]. That study solved the state-mismatch problem by constructing a separate fingerprint database for each environmental state and selecting the corresponding database in the online phase by a state classifier [16]. However, this solution left a clear scalability limitation: if H structural elements each have two possible states, the number of state-specific databases is 2^H. For example, $H = 10$ already corresponds to 1024 complete offline surveys, which is difficult to support in an actual deployment.

DOI: 10.13164/re.2026.0407

Therefore, the present paper extends that multi-fingerprint framework by retaining the state-aware localization premise while changing its most expensive component: instead of measuring every state-specific fingerprint database, fingerprints are estimated for environmental states that have not been physically surveyed. The proposed CoStateLoc (Compositional State-Conditioned Localization) framework constructs unseen-state fingerprints from the measured baseline state, all single-factor states, and a limited number of dual-factor states. The underlying modeling assumption is that the RSS variation caused by several structural elements can often be approximated by the superposition of single-factor perturbations and sparse pairwise interaction terms. In this way, CoStateLoc preserves the state-aware localization structure while avoiding exhaustive surveys over the whole state space. The present validation is a controlled mechanism study: the main experiments assume that the online environmental state is available, and the reported accuracy is obtained in reproducible simulated layouts rather than in a calibrated real building. This scope is intended to isolate the radio-map reconstruction mechanism before the framework is coupled with real-building measurement campaigns and state-identification hardware.

The main contributions of this paper can be summarized as follows:

- The unseen-state radio map reconstruction problem is formalized for variable indoor spatial environments. Different from conventional fingerprint matching studies, the research object is the construction of fingerprint databases for environmental states that are absent from the offline survey set.

- CoStateLoc is proposed as a compositional perturbation model that estimates unseen-state fingerprints from baseline, single-factor, and selected dual-factor state databases. The required number of state-specific surveys is reduced from 2^H to $1 + H + K$, where K is the selected dual-factor survey budget.

- A reproducible 2D geometric ray-tracing evaluation environment is built with coherent multipath combining, explicit material parameters, and state-dependent door configurations. This simulator provides controlled RSS data for comparing full-survey, incomplete-survey, and ablation methods under the same localization backend.

- The proposed method is evaluated with $H = 6$ doors across three geometrically different layouts. Under the adopted simulation model, the results show that CoStateLoc reduces the number of state-specific surveys by 65.6% while keeping the localization error close to the full-survey oracle and improving accuracy over the first-order additive baseline.

The remainder of this paper is organized as follows. Section 2 reviews related work. Section 3 formulates the incomplete-survey fingerprint generation problem. Section 4 presents the proposed CoStateLoc framework. Section 5 describes the ray-tracing evaluation environment. Section 6 gives the experimental setup, results, and discussion. Section 7 concludes the paper, and Section 8 states data and code availability.

2. Related Work

The first representative Wi-Fi fingerprint localization system, RADAR, used measured RF signal strength to estimate indoor user locations and established the offline-online framework followed by many later systems [3]. Probabilistic wireless local area network (WLAN) localization was then studied to describe RSS uncertainty, including early Bayesian RSS models and the Horus system [4], [9]. On this basis, KNN and WKNN methods became widely used because of their simple implementation and acceptable accuracy [5], [10]. Later studies further analyzed RSS statistical properties, AP selection, feature construction, machine learning, and deep learning to improve the matching relationship between RSS fingerprints and physical locations [6, 11, 12, 15, 17–19]. These methods mainly improve the online matching algorithm or the fingerprint representation, while the radio map is usually still assumed to correspond to the same environmental condition as the online measurement.

To reduce the cost of fingerprint database construction and maintenance, many studies have considered site-survey-free localization, radio-map update, crowdsourcing, and interpolation [20]. Crowdsourcing-based methods collect RSS data from ordinary mobile users and use them to build or update the radio map, thereby reducing manual survey workload [21–23]. Other studies update fingerprints when AP signals change or estimate fingerprints at unsurveyed locations from a limited number of collected points [24], [25]. These methods are valuable for reducing spatial sampling density or maintaining radio maps over time. However, their main target is the location dimension or temporal maintenance of the radio map. They do not directly solve the combinatorial growth caused by multiple structural elements whose states can change independently.

Missing radio-map entries can also be viewed through a completion perspective. Matrix completion estimates unobserved entries from low-rank structure [26], and tensor decompositions extend this idea to multi-way data arrays [27]. Recent radio-map learning studies have further used adversarial fingerprint learning, graph attention networks, conditional generative adversarial networks, and diffusion models to reconstruct or generate radio maps [28–31]. Graph neural networks have also been used to improve Wi-Fi localization with access point selection [32]. These methods show the value of modern learning-based radio-map modeling. However, the problem considered here is not random missing entries in a densely sampled array or spatial interpolation over unmeasured locations. The surveyed states are deliberately restricted to baseline, single-factor, and selected dual-factor configurations, and the target is to extrapolate to higher-order environmental state combinations. CoStateLoc therefore uses an explicit factorial perturbation structure rather than assuming only a global low-rank, graph-based, or generative latent representation.

Another line of work treats environmental variation as a domain shift problem. Transfer learning and domain adaptation attempt to map fingerprints collected under different conditions into a common feature space or adapt a trained localization model to a target domain [33], [34]. Such methods are useful when the source and target domains have related distributions and when some target-domain information can be obtained. Nevertheless, for door and partition state changes, the target domain is not a single continuous drift but a set of discrete structural combinations. If each combination is treated as a separate target domain, the amount of required calibration data still grows rapidly with the number of variable elements.

Propagation-model and ray-tracing methods provide another way to analyze RSS variation. Classical indoor propagation studies and standards describe free-space loss, indoor path loss, wall penetration, reflection, and multipath fading mechanisms [35–39]. Ray-tracing methods can further simulate site-specific multipath propagation in a given geometric environment [40], and differentiable radio-propagation platforms have recently made such modeling more accessible [41]. These methods help explain why opening or closing a door can change RSS fingerprints. However, pure model-based prediction often depends on detailed material parameters and geometric calibration. In this paper, ray tracing is used as a controlled evaluation environment, while the proposed CoStateLoc model itself estimates state perturbations directly from surveyed fingerprint databases.

The prior studies most closely related to the present work can be grouped according to their research objectives. One group focused on improving fingerprint-localization robustness, feature construction, or matching accuracy when the fingerprint database for the target condition was already available [15], [17]. Another group studied multi-fingerprint localization in variable spatial environments, showing that complex dynamic environments can produce distinguishable fingerprint patterns and that a state-aware system can select a corresponding state-specific database [16], [42]. These studies motivated state-aware fingerprint localization, but they still required the state-specific databases to be constructed in advance. In contrast, this paper addresses the radio-map construction problem: it reconstructs fingerprint databases for unseen environmental states from a limited set of surveyed states. Instead of constructing every state-specific database independently, CoStateLoc generates unseen-state fingerprints by composing measured single-factor effects and selected pairwise interactions, so that the survey burden is linked to the number and interaction structure of variable elements rather than to all 2^H state combinations.

3. Problem Formulation

Consider an indoor environment with N access points (APs) and M reference points (RPs) arranged in a grid. The setting follows the variable-spatial-state assumption used in the previous multi-fingerprint localization framework [16], but the objective is different. The earlier framework assumed that the fingerprint database of each state had been surveyed. Here, the environment still contains H variable structural elements (e.g., doors, partitions, movable walls), each of which can be in one of two states: open (1) or closed (0), but only a subset of state-specific databases is available. The environmental state is represented by a binary vector:

$$\mathbf{s} = [s_1, s_2, \ldots, s_H] \in \{0,1\}^H \tag{1}$$

yielding a total of $S = 2^H$ possible states.

For each state $\mathbf{s}$, the fingerprint database $\mathbf{F}(\mathbf{s}) \in \mathbb{R}^{M\times N}$ contains the RSS values from all N APs measured at each of the M RPs:

$$\mathbf{F}(\mathbf{s}) = [\mathbf{f}_1(\mathbf{s}), \mathbf{f}_2(\mathbf{s}), \ldots, \mathbf{f}_N(\mathbf{s})] \tag{2}$$

where $\mathbf{f}_j(\mathbf{s}) \in \mathbb{R}^M$ is the RSS vector of AP j across all RPs under state $\mathbf{s}$.

Let $\mathcal{S}_{\text{survey}} \subset \{0,1\}^H$ denote the set of states that have been physically surveyed, and $\mathcal{S}_{\text{unseen}} = \{0,1\}^H \setminus \mathcal{S}_{\text{survey}}$ denote the unseen states. The all-closed state is denoted as $\mathbf{s}_0 = [0, 0, \ldots, 0]$. In the complete multi-fingerprint setting, every state-specific database is surveyed, so $|\mathcal{S}_{\text{survey}}| = 2^H$. In this paper, only a subset of state-specific databases is available, i.e., $|\mathcal{S}_{\text{survey}}| \ll 2^H$. Given the surveyed fingerprints $\{\mathbf{F}(\mathbf{s})|\mathbf{s} \in \mathcal{S}_{\text{survey}}\}$, the task is to generate $\hat{\mathbf{F}}(\mathbf{s})$ for every unseen state $\mathbf{s} \in \mathcal{S}_{\text{unseen}}$ and use the generated database to localize online RSS observations. The method-specific choice of $\mathcal{S}_{\text{survey}}$ is described in Sec. 4. The localization performance is evaluated by the mean positioning error:

$$e = \frac{1}{|\mathcal{S}_{\text{unseen}}|} \sum_{\mathbf{s}\in\mathcal{S}_{\text{unseen}}} \frac{1}{M} \sum_{i=1}^{M} \|\hat{\mathbf{p}}_i(\mathbf{s}) - \mathbf{p}_i\| \tag{3}$$

where $\hat{\mathbf{p}}_i(\mathbf{s})$ is the estimated position of RP i under state $\mathbf{s}$, and $\mathbf{p}_i$ is the true position.

4. Proposed CoStateLoc Framework

CoStateLoc is a concrete incomplete-survey solution for the problem defined in Sec. 3. Its survey set contains the baseline state $\mathbf{s}_0$, all single-factor states $\mathbf{e}_h$ in which only element h is open, and K selected dual-factor states $\mathbf{e}_{hq}$ in which elements h and q are simultaneously open. The number of surveyed states is therefore $1 + H + K$, where $K \leq C(H, 2)$, rather than the exhaustive 2^H states. From these surveyed databases, CoStateLoc constructs the fingerprint database of an unseen environmental state. The overall workflow is shown in Fig. 1, where partial state surveys, effect extraction, unseen-state radio map reconstruction, and

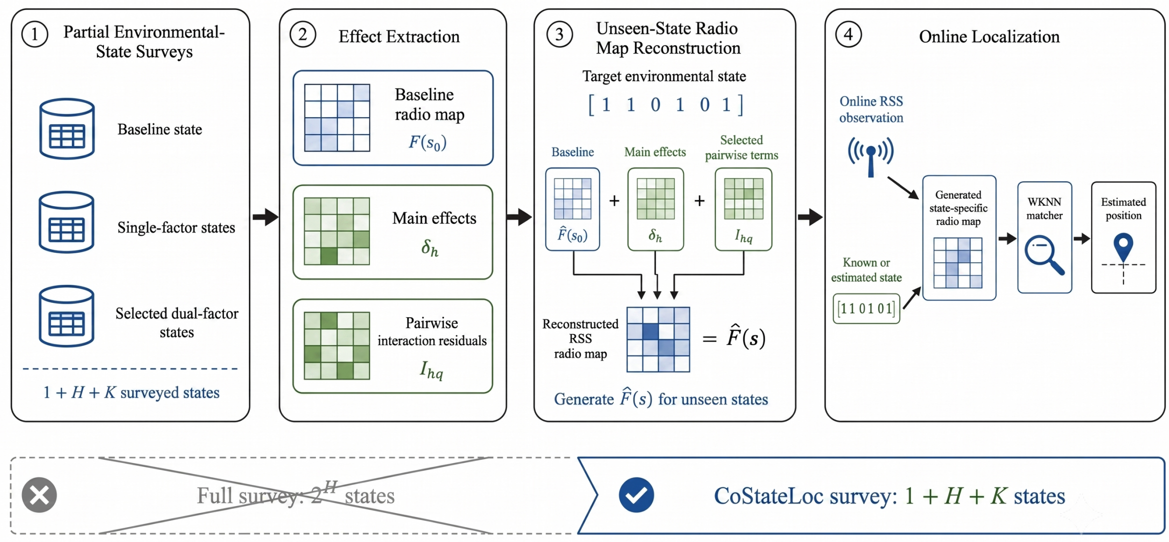

Fig. 1. Overview of the proposed CoStateLoc framework. Partial environmental-state surveys are used to extract baseline, main-effect, and pairwise-interaction components, which are then composed to reconstruct unseen-state radio maps for WKNN localization.

online localization are separated to make the role of the reconstructed state-specific radio map explicit.

Following the main-effect and interaction terminology commonly used in factorial experimental analysis [43], the fingerprint of state $\mathbf{s}$ is modeled as:

$$\hat{\mathbf{F}}(\mathbf{s}) = \mathbf{F}(\mathbf{s}_0) + \sum_{h=1}^{H} s_h \boldsymbol{\delta}_h + \sum_{h<q} s_h s_q \mathbf{I}_{hq} \tag{4}$$

where $\mathbf{F}(\mathbf{s}_0)$ is the baseline fingerprint database, $\boldsymbol{\delta}_h = \mathbf{F}(\mathbf{e}_h) - \mathbf{F}(\mathbf{s}_0)$ is the single-factor perturbation caused by element h, and $\mathbf{I}_{hq}$ is the pairwise interaction between elements h and q. No regression coefficient is fitted in this model. Each term is obtained by direct subtraction from surveyed state databases, so the reconstruction is fully determined once the survey set is fixed. For a surveyed dual-factor state, the interaction term is computed as the residual that cannot be explained by the two single-factor perturbations:

$$\mathbf{I}_{hq} = \mathbf{F}(\mathbf{e}_{hq}) - \mathbf{F}(\mathbf{s}_0) - \boldsymbol{\delta}_h - \boldsymbol{\delta}_q. \tag{5}$$

The interaction terms are not assumed to be dense. In indoor propagation, two elements are likely to interact when they affect common AP-RP paths. This gives a practical survey rule based only on known geometry. The rule is a heuristic design choice of this paper, and its effect is evaluated by the survey-budget experiment in Sec. 6. Let $\mathbf{c}_h \in \mathbb{R}^2$ denote the center coordinate of variable element h. The pair distance is:

$$d_{hq} = \|\mathbf{c}_h - \mathbf{c}_q\|_2. \tag{6}$$

All $C(H,2)$ pairs are sorted by d_{hq}. The K closest pairs are surveyed as dual-factor states, where K is the dual-factor survey budget and is distinct from the WKNN neighbor number k. For unselected pairs outside $\mathcal{Q}$, $\mathbf{I}_{hq}$ is set to zero. Because the ranking uses only element coordinates, it can be applied before dual-factor RSS measurements are collected.

Component	Cost formula
Surveyed maps	$S = O((1+H+K)MN)$
Main effects	$T = O(HMN),\ S = O(HMN)$
Pairwise terms	$T = O(KMN),\ S = O(KMN)$
One reconstructed map	$T = O((H+K)MN),\ S = O(MN)$
Cache U maps	$T = O(U(H+K)MN),\ S = O(UMN)$

Tab. 1. Computational complexity and memory requirement of CoStateLoc.

H	2^H	$1+H+C(H,2)$	Saving
6	64	22	65.6%
8	256	37	85.5%
10	1024	56	94.5%
12	4096	79	98.1%

Tab. 2. Survey-count scaling under the all-pair CoStateLoc design.

The computational cost of CoStateLoc is determined by the number of RPs M, APs N, variable elements H, selected dual-factor states K, and reconstructed unseen states U. Let T denote computational time and S denote storage. Table 1 summarizes the main cost formulas. The model can either reconstruct an unseen-state radio map on demand, which needs only one temporary $M \times N$ database, or cache all U reconstructed databases when repeated online queries for many states are expected.

The survey-count scalability follows directly from the factorial structure. If all pairwise interactions are surveyed, the required number of surveyed states is $1 + H + C(H,2)$; if only a subset of pairs is selected, it is $1 + H + K$. Table 2 gives the all-pair count for several values of H. This table is an analytic survey-count comparison, not an additional propagation experiment. It shows that the survey saving increases rapidly as H grows, because the exhaustive multi-fingerprint requirement is exponential whereas the all-pair CoStateLoc design is quadratic.

The complete offline reconstruction and online localization procedure is summarized in Algorithm 1.

Algorithm 1. Proposed CoStateLoc framework.

Require: Structural element center coordinates $\{\mathbf{c}_h\}_{h=1}^{H}$, dual-factor survey budget K, online RSS observation $\mathbf{r} \in \mathbb{R}^N$, and current environmental state $\mathbf{s} \in \mathcal{S}_{\text{unseen}}$.
Ensure: Estimated user location $\hat{\mathbf{p}}$.

```
Offline Surveying Phase:
Survey the baseline state s_0 = [0, ..., 0] to obtain baseline fingerprint database F(s_0).
for each variable element h = 1 to H do
    Survey single-factor state e_h (where only element h is open) to obtain database F(e_h).
    Compute single-factor perturbation (main effect):
    δ_h = F(e_h) − F(s_0).
end for
Compute spatial distance d_hq = ||c_h − c_q||_2 for all pairs 1 ≤ h < q ≤ H.
Sort all C(H, 2) pairs in ascending order of d_hq.
Select the top-K closest pairs as the dual-factor survey set Q.
for each selected pair (h, q) ∈ Q do
    Survey dual-factor state e_hq (where both elements h and q are open) to obtain database F(e_hq).
    Compute pairwise interaction term:
    I_hq = F(e_hq) − F(s_0) − δ_h − δ_q.
end for
for each remaining pair (h, q) ∉ Q do
    Set interaction term I_hq = 0.
end for
Online Reconstruction & Localization Phase:
Predict fingerprint database F̂(s) for the unseen state s:
F̂(s) = F(s_0) + Σ_{h=1}^{H} s_h δ_h + Σ_{(h,q)∈Q} s_h s_q I_hq.
Match online RSS observation r against F̂(s) using WKNN.
return Estimated user position p̂.
```

During online localization, the current environmental state $\mathbf{s}$ is assumed to be known or estimated by a state-identification module. This assumption follows the state-aware localization premise of the previous multi-fingerprint framework, but it requires an additional deployment component: a practical system must obtain the door, partition, or obstacle state before selecting the generated radio map. In deployment, this information may come from door sensors, building-management systems, vision-based room-state recognition, or a fingerprint-based state classifier such as the one used in the earlier multi-fingerprint framework [16]. These sensing choices are outside the main contribution of the present paper. In the main experiments, the state source is kept fixed so that the effect of incomplete state surveys can be isolated. The additional state-label-error experiment in Sec. 6 then examines how the method behaves when the provided state is occasionally wrong. Given an online RSS observation $\mathbf{r} \in \mathbb{R}^N$, CoStateLoc first reconstructs $\hat{\mathbf{F}}(\mathbf{s})$ using (4) and then applies the standard weighted k-nearest-neighbor (WKNN) fingerprint matcher [5], [10]:

$$\hat{\mathbf{p}} = \sum_{i \in \mathcal{N}_k} w_i \mathbf{p}_i, \quad w_i = \frac{1/\|\mathbf{r} - \hat{\mathbf{f}}_i\|}{\sum_{j \in \mathcal{N}_k} 1/\|\mathbf{r} - \hat{\mathbf{f}}_j\|} \tag{7}$$

where $\mathcal{N}_k$ is the set of k nearest reference points in the predicted database, and $\hat{\mathbf{f}}_i$ is the predicted RSS vector at RP i.

5. Ray-Tracing Evaluation

To make the RSS generation process repeatable, this paper uses a 2D geometric ray-tracing simulator as a controlled radio-map generator. The simulator follows the standard path-loss and image-method ray-tracing procedure used in indoor radio propagation modeling [36], [40]. It is not calibrated to a particular building; instead, it provides the same RSS field to all compared methods so that the effect of incomplete state surveys can be isolated. The layout geometry, AP and RP coordinates, door apertures, material placeholders, survey-state definitions, and random seeds are fixed in the implementation, so the same configuration deterministically regenerates the same offline radio maps.

For each AP-RP pair under a given environmental state, three types of paths are considered: the direct path, all valid single-bounce reflected paths, and all valid double-bounce reflected paths. The reflection points are computed deterministically by mirroring the AP across wall segments and checking whether the resulting path intersects the finite wall segment. A path segment crossing a closed wall or a closed door accumulates wall penetration loss. If the crossing point lies inside an open door aperture, no wall penetration loss is added at that crossing. The same open door aperture is also removed from the set of valid reflecting surfaces, so an opened door affects both penetration and reflection paths.

For a path l with length d_l, wall penetration loss $L_{\mathrm{w},l}$, and $n_{r,l}$ reflections, the complex field contribution is:

$$E_l = \frac{1}{d_l^{n/2}} 10^{-L_{\mathrm{w},l}/20} \Gamma^{n_{r,l}} \mathrm{e}^{-\mathrm{j}2\pi d_l/\lambda} \tag{8}$$

where n is the path-loss exponent, Γ is the reflection coefficient in amplitude, and λ is the wavelength. The distance-decay, penetration-loss, reflection-loss, and phase terms follow the narrowband link-budget and multipath representation used in wireless propagation analysis [35, 36, 38]. The total field is coherently summed as:

$$E_{\text{total}} = E_{\text{LOS}} + \sum_i E_{\text{refl},i} + \sum_j E_{\text{double},j} \tag{9}$$

where E_{LOS} is the line-of-sight (LOS) direct contribution, $E_{\text{refl},i}$ is the i-th single-bounce contribution, and $E_{\text{double},j}$ is the j-th double-bounce contribution. The received power is finally converted to RSS in dBm by:

$$P_{1\text{m}} = 10^{(P_\text{t} - 20\log_{10}(4\pi f/c))/10} \tag{10}$$

$$P_\text{r} = 10\log_{10}\left(P_{1\text{m}}|E_{\text{total}}|^2\right) \tag{11}$$

where P_t is the AP transmit power in dBm, f is the carrier frequency, and c is the speed of light. Equation (10) is the 1 m free-space reference-power form of the Friis transmission formula [35]. The value $P_{1\text{m}}$ is therefore the received power at the 1 m free-space reference distance expressed in mW. If numerical cancellation makes $P_{1\text{m}}|E_{\text{total}}|^2 < 10^{-20}$ mW, the RSS is clipped to −100 dBm. This clipping threshold is only a numerical floor for extremely small simulated powers; it is not a measured receiver-sensitivity parameter. This implementation makes the generated fingerprint database deterministic for a fixed layout, state vector, and parameter set. The default offline radio maps are noise-free simulated fields, while Gaussian measurement noise is added only when online RSS observations are generated for localization testing. This is an idealized offline-survey setting and is treated as a limitation when interpreting the results.

The use of coherent summation in (9) means that the RSS field contains constructive and destructive multipath interference. At 2.4 GHz, $\lambda \approx 12.5$ cm, and therefore small path-length differences can produce fast fading [38]. This setting is intentionally a difficult benchmark for fingerprint generation. It is not intended to replace a calibrated full-wave or three-dimensional (3D) ray-tracing tool; instead, it provides a controlled and reproducible way to test whether the proposed compositional model can recover state-dependent RSS changes under nonlinear multipath conditions.

The simulator is therefore a deliberate abstraction rather than a complete representation of a measured building. It considers a single 2.4 GHz carrier, planar walls, binary door apertures, wall penetration, specular reflection, and coherent multipath combining. It does not model 5/6 GHz operation, diffraction, diffuse scattering, furniture and equipment, moving people, device heterogeneity, floor-ceiling effects, full 3D propagation, partially open doors, or the attenuation of an opened door leaf lying close to a wall. These factors are important for field deployment, but adding them in the present stage would mix the radio-map reconstruction question with site-specific calibration and sensing variables. The controlled simulator is used to test whether the proposed state-composition mechanism is useful when all methods face the same geometry, propagation model, AP layout, test states, and noise assumptions. Real-building measurements, multi-band evaluation, and independent 3D ray-tracing tools are treated as the next validation stage.

6. Experiments

6.1 Experimental Setup

Table 3 lists the parameters used in the experiments. The propagation-related values are selected from commonly used indoor ranges rather than tuned for CoStateLoc. The 2.4 GHz carrier is the standard Wi-Fi band used in many RSS fingerprint systems [3], [10]; 5/6 GHz operation is not evaluated in this paper and is included in the future validation plan. The path-loss exponent and wall loss are within the indoor ranges reported in classical indoor propagation measurements and ITU indoor planning recommendations [37], [39]. The reflection coefficient is treated as a fixed material placeholder in the image-method model [36], [40]; it is reported for reproduction and is not optimized. Parameters that define the controlled simulation design, such as AP power, RP spacing, Monte Carlo repetitions, and the random seed, are fixed for all methods and are not presented as literature-derived optimal values. The hardware and software platform is also reported only for reproducing the runtime measurements, not as a hardware-independent efficiency claim.

Three controlled layouts are used to reduce dependence on a single geometry. They are synthetic evaluation layouts rather than replicas of specific measured buildings. Each layout contains $H = 6$ variable doors and therefore $2^6 = 64$ possible environmental states. Layout A is a 32×10 m corridor-like room divided by six parallel vertical walls, each with a door. Seven APs are distributed along the room, as shown in Fig. 2. This layout creates repeated cross-wall propagation paths and is expected to have stronger interaction effects. Layout B is a 20×16 m mixed-wall environment with three vertical and three horizontal wall segments, as shown in Fig. 3. Its geometry is less aligned, and the variable doors are more spatially separated. Layout C is a 20×16 m asymmetric environment with staggered vertical and horizontal partitions and two oblique wall segments, as shown in Fig. 4. Its nonuniform AP placement and oblique propagation boundaries differ from both the parallel structure of Layout A and the orthogonal mixed structure of Layout B. All three layouts have an area of 320 m^2. RPs are placed on a 2.0 m grid, yielding 80 RPs in each layout.

Parameter	Value and basis
Frequency	2.4 GHz Wi-Fi band [3], [10]
AP transmit power	20 dBm, fixed equal-power AP setting
Path types	LOS, single reflection, double reflection [36], [40]
Path-loss exponent	2.8, indoor range [37], [39]
Wall attenuation	15 dB per closed wall or door [37], [39]
Reflection coefficient	0.7 amplitude, exact value fixed in this paper; image-method basis in [36], [40]
Online noise std.	3.0 dB controlled default, varied over 1–7 dB; Gaussian RSS-fluctuation basis in [12]
WKNN k	3, fixed for all methods; WKNN principle in [5], [10]
Monte Carlo runs	30 independent online noise realizations; random seed 42
RP spacing	2.0 m, fixed controlled grid setting
Runtime platform	AMD Ryzen 5 9600X processor, 32 GB memory, Python 3.14.2

Tab. 3. Simulation and evaluation parameters.

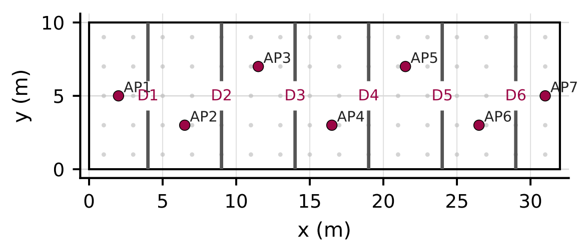

Fig. 2. Simulation layout A with six variable doors, seven APs, and reference points shown as gray dots.

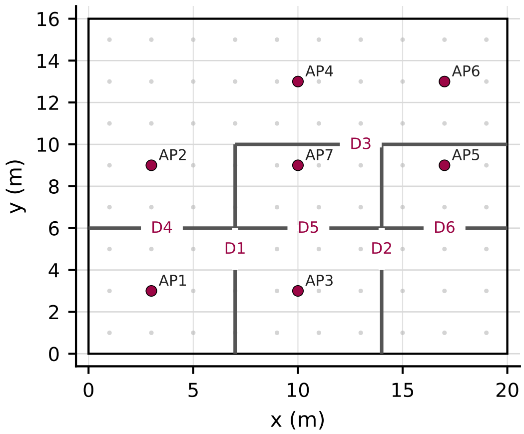

Fig. 3. Simulation layout B with mixed vertical and horizontal walls. D1–D6 denote six variable apertures, AP1–AP7 denote access points, and gray dots denote reference points.

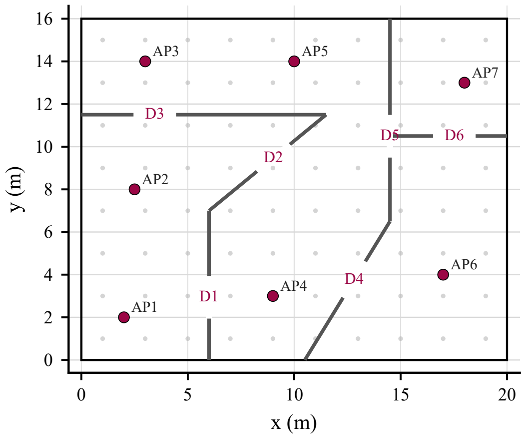

Fig. 4. Simulation layout C with asymmetric staggered and oblique partitions. D1–D6 denote six variable apertures, AP1–AP7 denote access points, and gray dots denote reference points.

Method	States used	Database used for an unseen state
OracleFull	64	True state database; full-survey upper bound
BaseOnly	1	Baseline database $\mathbf{F}(\mathbf{s}_0)$
FirstOrder	7	Baseline plus single-factor perturbations
NearestObs	22	Nearest surveyed state in Hamming distance
RandomSurvey	22	NearestObs after random state selection
KernelState	22	Hamming-RBF kernel regression over state vectors
CoStateLoc	22	Baseline, single-factor, and pairwise terms

Tab. 4. Compared fingerprint database construction methods.

For all three layouts, the default CoStateLoc survey set contains the baseline state, all six single-factor states, and all 15 dual-factor states. This gives 22 surveyed states, or 34.4% of all possible states. The remaining 42 states, all with at least three open doors, are not used for database construction and are reserved for testing. In the survey-budget experiment, the number of dual-factor states is reduced according to the spatial proximity rule in (6).

All compared methods use the same WKNN localizer in (7); they differ only in how the fingerprint database for an unseen state is obtained. Table 4 summarizes the database construction rules, and the exact comparison protocol is as follows.

- *OracleFull*: uses the true state-specific database $\mathbf{F}(\mathbf{s})$ for each test state. It is a full-survey upper bound with perfect state knowledge.
- *BaseOnly*: always uses the all-closed baseline database $\mathbf{F}(\mathbf{s}_0)$, measuring the error caused by ignoring environmental state changes.
- *FirstOrder*: uses the baseline database and all single-factor perturbations, but sets all pairwise terms in (4) to zero. It is a main-effect-only factorial model [43].
- *NearestObs*: selects the surveyed state with the minimum Hamming distance to the test state and reuses that surveyed database. It is a reproducible state-reuse baseline following the nearest-neighbor decision principle [44].
- *RandomSurvey*: randomly selects 22 surveyed states, with the baseline state forced to be included, and then applies the same NearestObs rule. The reported value is averaged over five random selections.
- *KernelState*: predicts an unseen state's full RSS map by Hamming radial-basis-function (RBF) kernel ridge regression over the binary state vector. Kernel ridge regression follows the dual kernel-regression principle [45], and kernel models have also been used in WLAN fingerprinting [18]. The length scale and ridge parameter are selected by leave-one-surveyed-state-out RSS reconstruction error.
- *CoStateLoc*: uses the baseline, six single-factor databases, and selected pairwise interaction terms computed by (5).

During localization testing, an online RSS observation at RP i under state $\mathbf{s}$ is generated as:

$$\mathbf{r}_i(\mathbf{s}) = \mathbf{f}_i(\mathbf{s}) + \boldsymbol{\epsilon}, \quad \epsilon_j \sim \mathcal{N}(0, \sigma^2) \tag{12}$$

where $\sigma = 3$ dB by default and the noise components of different APs are sampled independently. Gaussian RSS fluctuation is used here as a reproducible measurement-noise abstraction, following the common statistical treatment of RSS fingerprints [9], [12]; the exact value of σ is a controlled default and is varied in the noise-sensitivity experiment rather than tuned for one method. Three metrics are reported. The mean localization error is the Euclidean distance between the estimated and true RP positions averaged over all test states, RPs, and Monte Carlo runs. The P90 error is the 90th percentile of the same localization error distribution. The RSS reconstruction root mean square error (RMSE) is computed as:

$$\mathrm{RMSE_{RSS}} = \sqrt{\frac{1}{|\mathcal{S}_{\mathrm{unseen}}|MN} \sum_{\mathbf{s}\in\mathcal{S}_{\mathrm{unseen}}} \|\hat{\mathbf{F}}(\mathbf{s}) - \mathbf{F}(\mathbf{s})\|_F^2}. \quad (13)$$

To check the consequence of imperfect state information, an additional sensitivity test is performed in Layout A. With probability p_s, the perceived online state is replaced by a one-bit-flipped state label, while the online RSS observation is still generated from the true state. This setting represents a mild state-identification error in which the state module confuses one structural element, and it is used only to quantify sensitivity to state-label errors rather than to solve state recognition.

To test the idealized noise-free offline-survey assumption, another Layout A sensitivity test perturbs only the surveyed databases before model construction:

$$\tilde{\mathbf{F}}(\mathbf{s}) = \mathbf{F}(\mathbf{s}) + \boldsymbol{\eta}, \quad \eta_{ij} \sim \mathcal{N}(0, \sigma_{\mathrm{off}}^2). \quad (14)$$

The true unseen-state radio maps used for online testing are not perturbed by $\boldsymbol{\eta}$. Five independent offline-noise realizations are used for each σ_{off}. Because a pairwise interaction term is computed from four surveyed databases, its noise variance is amplified. Therefore, this sensitivity test also reports a noise-aware variant, denoted CoStateLoc-S, which shrinks each observed interaction term by:

$$\tilde{\mathbf{I}}_{hq} = \alpha_{hq}\mathbf{I}_{hq}, \quad \alpha_{hq} = \max\left(0, \frac{\bar{I}_{hq}^2 - 4\sigma_{\mathrm{off}}^2}{\bar{I}_{hq}^2}\right) \quad (15)$$

where $\bar{I}_{hq}^2 = \|\mathbf{I}_{hq}\|_F^2/(MN)$. This variant is used only to examine how interaction terms should be regularized when offline fingerprints are noisy.

6.2 Results and Discussion

Before comparing localization accuracy, the simulated scenarios are first checked for the state-induced fingerprint shift that motivates this work. Figure 5 shows a representative example in Layout A. When doors D1 and D2 are opened, the AP1 RSS field changes by 8.6 dB on average and up to 36.2 dB across reference points. This result shows that the tested structural states generate materially different radio maps; therefore, the use of a mismatched fingerprint database can affect localization in this setting.

Figures 6 and 7(a) report the main localization performance. OracleFull gives the full-survey upper bound because it uses the true state-specific database for each test state. Its mean errors are 1.43 m, 1.02 m, and 1.26 m in Layouts A, B, and C, respectively. CoStateLoc uses only 22 surveyed states and obtains 1.61 m, 1.06 m, and 1.27 m. The corresponding gaps to OracleFull are 0.18 m, 0.04 m, and 0.015 m, while 65.6% of the state-specific surveys are avoided.

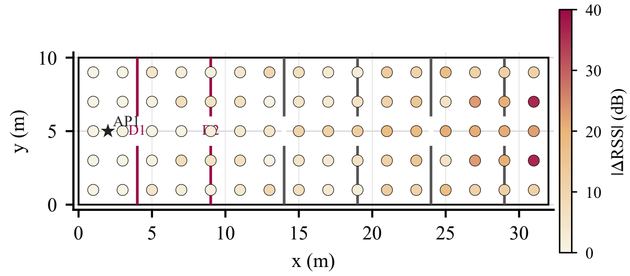

Fig. 5. Representative RSS fingerprint shift in Layout A. Point colors show the absolute AP1 RSS change between the all-closed baseline and the state where doors D1 and D2 are open.

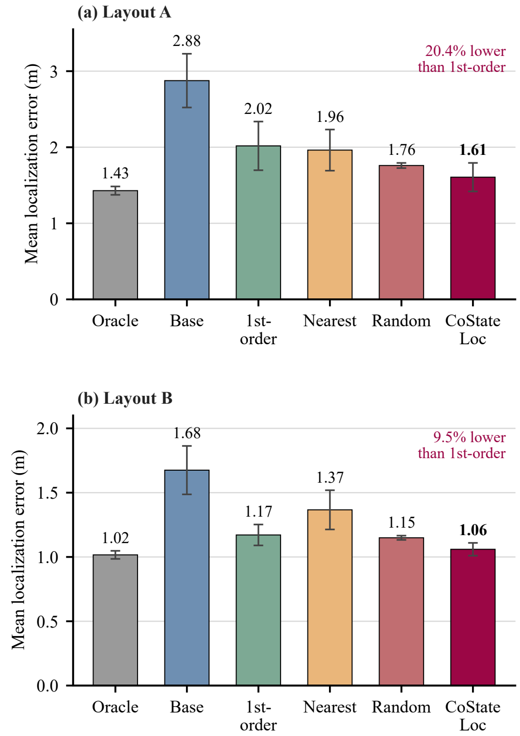

Fig. 6. Mean localization error on unseen states in (a) Layout A and (b) Layout B with OracleFull reference.

Among the incomplete-survey methods, CoStateLoc has the lowest mean error in all three layouts. Compared with FirstOrder, the error decreases from 2.02 m to 1.61 m in Layout A, from 1.17 m to 1.06 m in Layout B, and from 1.38 m to 1.27 m in Layout C. The corresponding improvements are 20.4%, 9.5%, and 7.8%. For the significance check, the paired samples are the 42 unseen-state mean errors, and the test statistic is $t = \bar{d}/(s_d/\sqrt{42})$, where d is the state-level error difference between FirstOrder and CoStateLoc. Following the paired-comparison procedure commonly used in experimental analysis [43], the test uses 41 degrees of freedom. It gives $t = 12.46$, 13.12, and 9.94 in Layouts A, B, and C, respectively, with two-sided $p < 0.001$ in each layout. The paired standardized effect sizes $d_z = t/\sqrt{42}$ are 1.92, 2.02, and 1.53. The approximate 95% confidence intervals for the FirstOrder–CoStateLoc mean-error reduction are 0.34–0.48 m, 0.09–0.13 m, and 0.086–0.129 m, respectively. The larger gain in Layout A is consistent with the

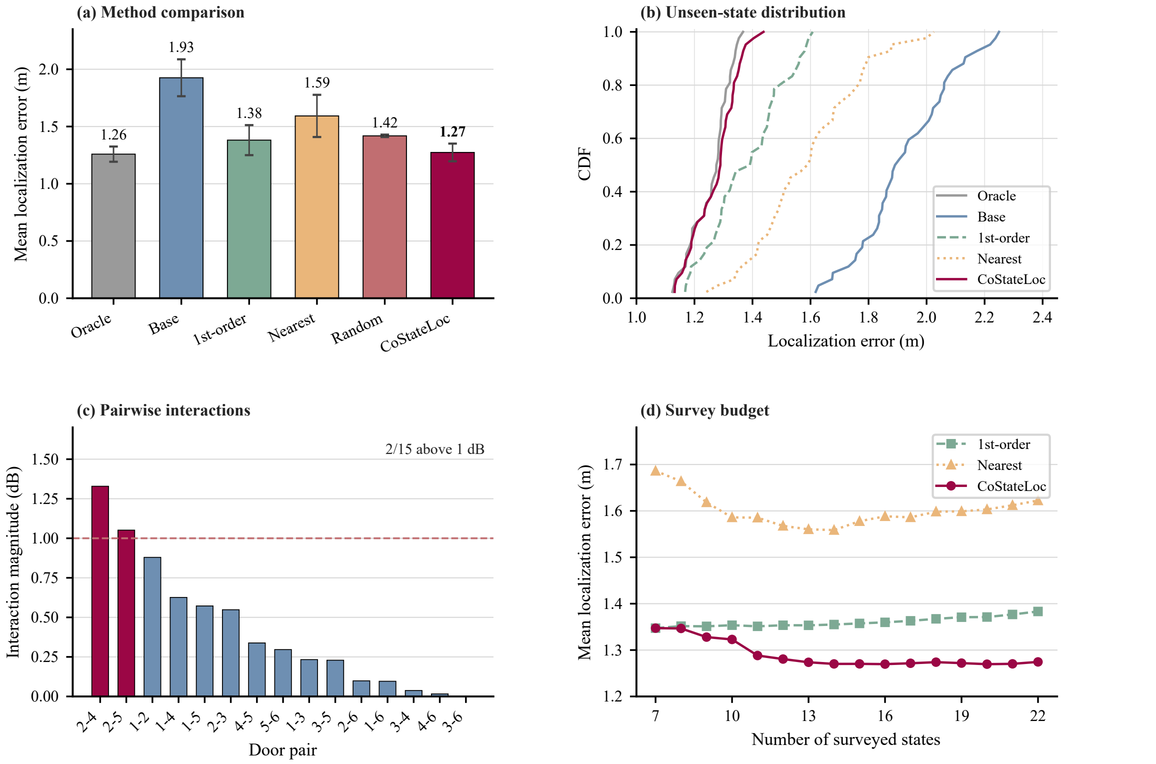

Fig. 7. Additional validation in the asymmetric Layout C: (a) mean localization error across the principal methods, (b) cumulative distribution of unseen-state mean errors, (c) pairwise interaction magnitudes, and (d) localization error under the spatial proximity survey-budget rule.

geometry in Fig. 2: parallel walls repeatedly intersect AP-RP paths, so two opened doors can create a propagation condition that is not reproduced by simply adding their single-door effects. Layouts B and C have fewer strong interactions, so the first-order model is already stronger. The positive paired differences nevertheless show that the pairwise terms remain useful in both geometries.

Table 5 further compares CoStateLoc with KernelState, a state-conditioned generator that uses the same 22 surveyed states but does not assume the main-effect plus pairwise-interaction structure. KernelState obtains mean localization errors of 1.82 m, 1.28 m, and 1.55 m in Layouts A, B, and C, while CoStateLoc obtains 1.61 m, 1.06 m, and 1.27 m. The corresponding global RSS RMSE values are 4.31, 3.72, and 3.71 dB for KernelState and 3.50, 1.65, and 1.57 dB for CoStateLoc. Thus, the explicit interaction decomposition is more accurate than smooth kernel interpolation over binary state labels in the three controlled layouts.

Figure 8 reports the global RSS reconstruction RMSE defined in (13). This metric is independent of the WKNN matching step and directly measures how well each method reconstructs the unseen-state fingerprint database. The corresponding global RMSE and mean absolute error (MAE) values are listed in Tab. 6. CoStateLoc has the lowest reconstruction error among the incomplete-survey methods in all three layouts. Relative to FirstOrder, its global RMSE is reduced by 36.1%, 51.0%, and 48.0% in Layouts A, B, and C, respectively. Thus, the localization gains in Figs. 6 and 7(a) are accompanied by direct improvements in radio-map reconstruction.

Layout	Method	Mean error (m)	RSS RMSE (dB)
A	KernelState	1.82	4.31
A	CoStateLoc	1.61	3.50
B	KernelState	1.28	3.72
B	CoStateLoc	1.06	1.65
C	KernelState	1.55	3.71
C	CoStateLoc	1.27	1.57

Tab. 5. Comparison with the Hamming-RBF KernelState generator baseline under the same 22-state survey protocol.

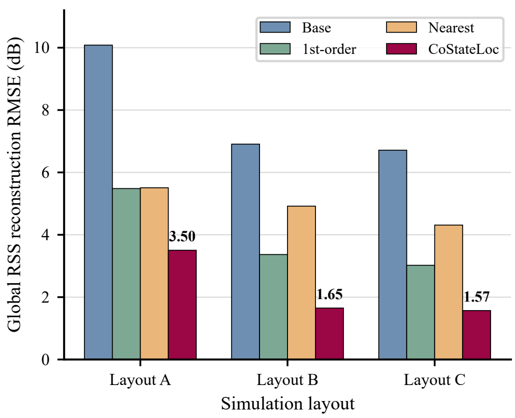

Fig. 8. Global RSS reconstruction RMSE on unseen states in Layouts A, B, and C.

Layout	Method	RMSE (dB)	MAE (dB)
A	BaseOnly	10.08	6.33
A	FirstOrder	5.48	2.42
A	NearestObs	5.51	2.68
A	CoStateLoc	3.50	0.93
B	BaseOnly	6.91	3.76
B	FirstOrder	3.37	0.97
B	NearestObs	4.92	2.04
B	CoStateLoc	1.65	0.26
C	BaseOnly	6.71	3.77
C	FirstOrder	3.02	0.78
C	NearestObs	4.31	1.74
C	CoStateLoc	1.57	0.14

Tab. 6. RSS reconstruction metrics on unseen states.

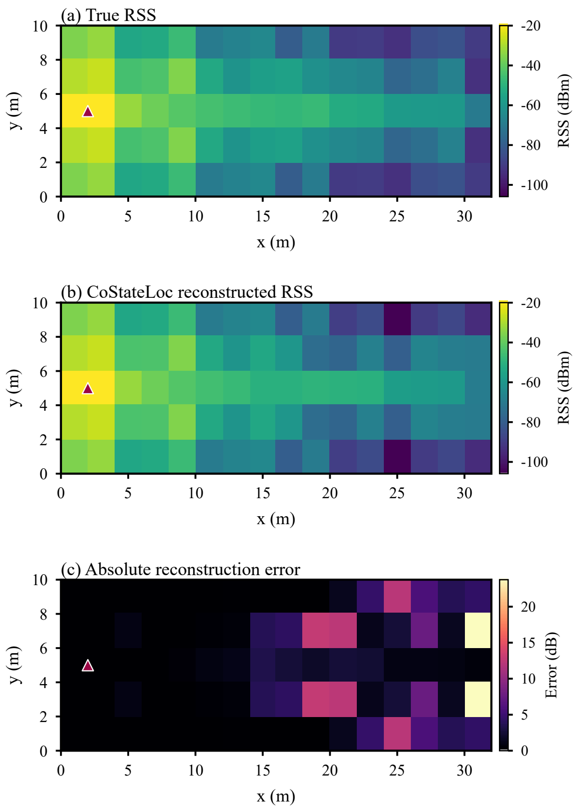

Fig. 9. Representative radio-map reconstruction for Layout A, AP1, and unseen state 111000: (a) true RSS, (b) CoState-Loc reconstructed RSS, and (c) absolute reconstruction error. The triangle denotes AP1.

Figure 9 provides a spatial comparison for Layout A, AP1, and unseen state 111000, in which D1–D3 are open and D4–D6 are closed. The reconstructed map preserves the broad RSS gradient from AP1 toward the far end of the layout. Its mean absolute reconstruction error is 2.76 dB. The maximum absolute error is 23.75 dB and occurs in localized regions near the far-right side, where coherent multipath fading produces sharp spatial variations. This example complements the aggregate values in Tab. 6: the compositional model captures the large-scale state-dependent field while retaining localized errors that are not represented by the second-order truncation.

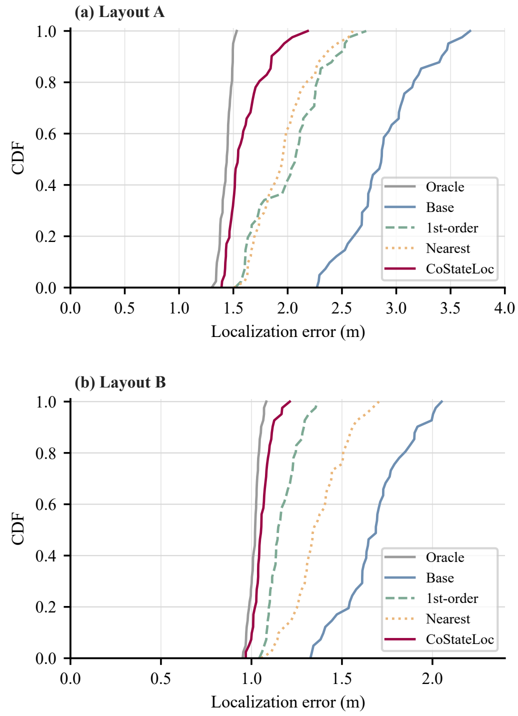

Fig. 10. CDF of unseen-state mean localization errors in (a) Layout A and (b) Layout B.

Layout	Method	Median (m)	Max. (m)	Success rate (%)
A	BaseOnly	2.68	11.34	16.0/37.0/57.6
A	FirstOrder	1.74	9.50	25.2/58.8/80.6
A	NearestObs	1.73	10.34	25.1/60.0/81.9
A	CoStateLoc	1.47	8.12	30.9/70.9/89.5
B	BaseOnly	1.46	14.24	29.9/70.1/89.9
B	FirstOrder	1.11	9.02	43.4/89.2/98.8
B	NearestObs	1.23	13.61	36.7/81.1/95.3
B	CoStateLoc	1.00	9.33	50.0/92.6/99.1
C	BaseOnly	1.72	9.36	21.6/59.7/84.5
C	FirstOrder	1.23	7.59	36.8/79.8/94.4
C	NearestObs	1.38	10.02	31.4/72.9/90.7
C	CoStateLoc	1.15	6.29	39.7/84.3/96.7

Tab. 7. Additional localization distribution metrics under the same online test setting. The success-rate column gives the percentages within 1/2/3 m.

The cumulative distribution function (CDF) curves in Figs. 10 and 7(b) further show how the errors are distributed across unseen states. The CoStateLoc curve lies to the left of the other incomplete-survey methods over most of the CDF range in each layout. In Layout A, its P90 error is 3.07 m, compared with 4.06 m for FirstOrder and 3.98 m for NearestObs. In Layout B, the corresponding values are 1.87, 2.05, and 2.46 m. In Layout C, they are 2.30, 2.55, and 2.93 m. Table 7 gives additional point-error metrics computed under the same online test setting. CoStateLoc has the lowest median error and the highest success rates within 1/2/3 m among the incomplete-survey methods in all three layouts. The maximum-error column shows that the main gain appears in the central and high-probability portions of the error distribution rather than eliminating every isolated extreme. The tail reduction is most pronounced in Layout A because the pairwise terms correct several high-error coupled states that the first-order and state-reuse baselines cannot represent.

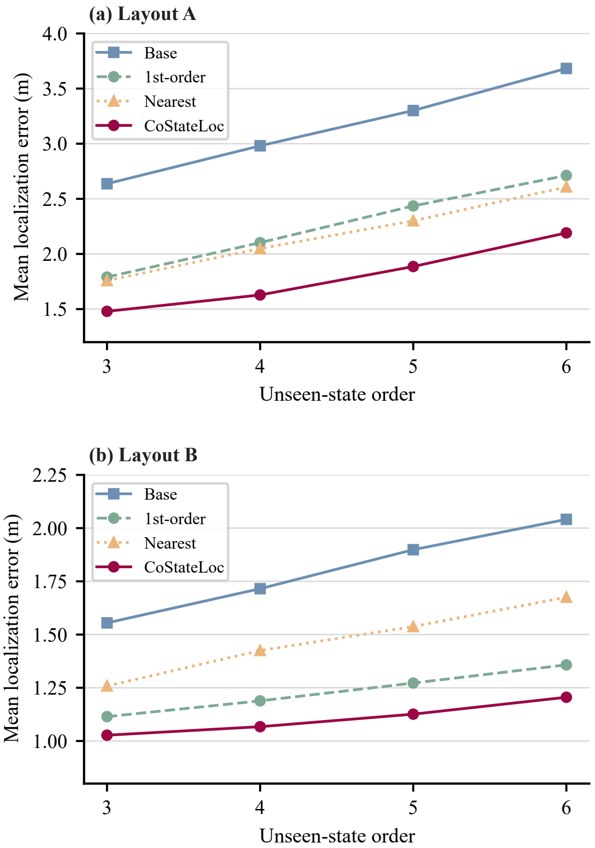

Fig. 11. Mean localization error by unseen-state order in (a) Layout A and (b) Layout B.

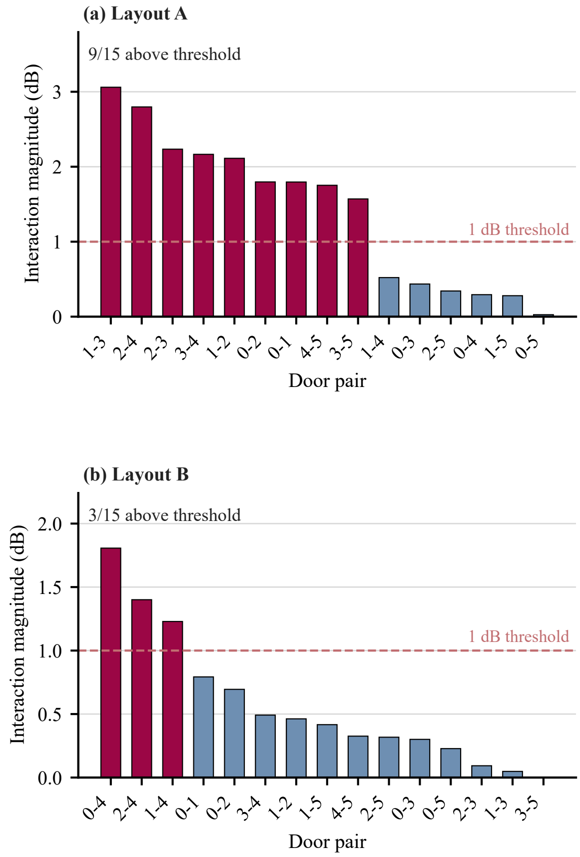

Fig. 12. Interaction term magnitudes for all 15 element pairs in (a) Layout A and (b) Layout B. Nine pairs in Layout A and three pairs in Layout B exceed the 1 dB descriptive marker.

Figure 11 further examines the effect of interaction order and survey budget on localization performance. For all methods, the localization error increases when more doors are simultaneously open, because higher-order states involve more unobserved door-state combinations and therefore require stronger generalization. CoStateLoc consistently achieves the lowest error at each order. At order 6, CoStateLoc obtains 2.19 m, 1.21 m, and 1.37 m in Layouts A, B, and C, whereas FirstOrder gives 2.71 m, 1.36 m, and 1.59 m, respectively. The improvement is most pronounced in Layout A, indicating that pairwise interaction terms are especially useful when the environment geometry induces stronger coupled propagation effects. The Layout C result confirms that the ordering is retained in the additional asymmetric geometry.

Figures 12 and 7(c) show the interaction magnitudes of all $C(6, 2) = 15$ door pairs. The 1 dB line is used only as a descriptive marker in this analysis; it is smaller than the default online noise standard deviation of 3 dB and is not used by the CoStateLoc reconstruction algorithm. Nine pairs in Layout A, three pairs in Layout B, and two pairs in Layout C exceed this marker. Therefore, interactions are not uniformly distributed across all pairs. They concentrate on a subset of geometrically related doors, which supports the use of a reduced dual-factor survey. The smaller number of strong pairs in Layout C is also consistent with its smaller improvement over FirstOrder.

The survey-budget curves in Figs. 13 and 7(d) use the deployable spatial proximity rule in (6). In Layout A, the CoStateLoc error decreases from 1.90 m with seven surveyed states to 1.61 m with 15 surveyed states. The latter setting uses the baseline, six single-factor states, and eight dual-factor states, i.e., only 23.4% of the 64 possible states. Adding more dual-factor states beyond this point brings little further improvement, and the 22-state setting remains at 1.61 m. In Layout B, CoStateLoc decreases from 1.14 m at seven surveyed states to about 1.06–1.07 m after 13 surveyed states. In Layout C, it decreases from 1.35 m at seven states to 1.27 m at 14 states and then remains near this level. This setting uses seven dual-factor surveys and 21.9% of all 64 states. The earlier plateaus in Layouts B and C are consistent with their smaller numbers of strong interaction pairs. FirstOrder changes only mildly because it does not use dual-factor measurements in reconstruction; the small drift is caused by the evaluated unseen-state set changing as additional dual-factor states are moved from the test set into the survey set. NearestObs remains more sensitive to which state databases happen to be available, because it reuses a single observed state rather than composing effects.

Table 8 gives an additional component ablation in Layout A. Different from Fig. 13, the Top-K dual-factor terms in this table are selected by their true interaction magnitudes.

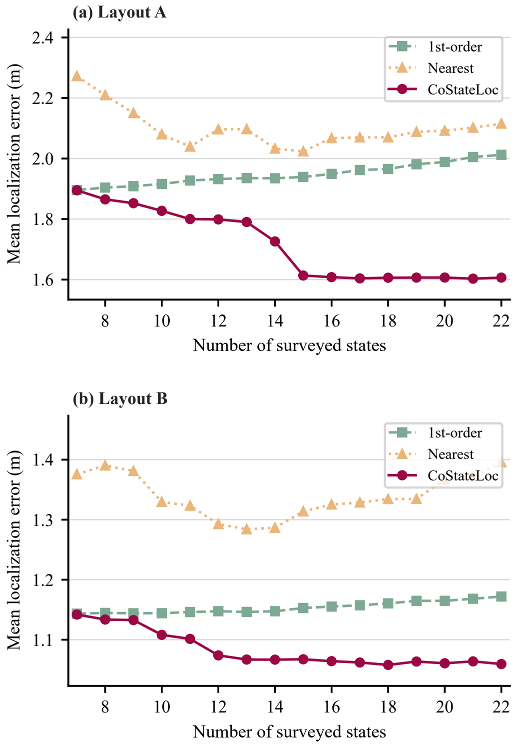

Fig. 13. Localization error vs. number of surveyed states in (a) Layout A and (b) Layout B under the spatial proximity heuristic.

Configuration	States used	Error (m)
BaseOnly	1	2.71
+ Single-factor (FirstOrder)	7	1.90
+ Top-3 dual-factor	10	1.69
+ Top-5 dual-factor	12	1.63
+ Top-7 dual-factor	14	1.61
+ All 15 dual-factor	22	1.61
NearestObs (all 22 states)	22	2.12

Tab. 8. Oracle component ablation: mean error (m) with different model components in Layout A.

This is an oracle analysis and is used only to isolate how much of the improvement is provided by the strongest interaction terms. The BaseOnly error is 2.71 m. After the six single-factor databases are used, the error decreases to 1.90 m, showing that main effects explain a large part of the state-dependent RSS change. Adding the three strongest dual-factor terms further reduces the error to 1.69 m, and the Top-7 setting already reaches the same 1.61 m level as all 15 dual-factor terms. NearestObs uses all 22 surveyed states but obtains 2.12 m, which is worse than FirstOrder with only seven states. Thus, collecting more state databases is not sufficient unless the information is combined through a suitable reconstruction model.

Figure 14 evaluates the robustness of different methods under increasing online RSS noise. The experiment is conducted in Layout A, which represents the stronger-interaction scenario. As the online noise standard deviation increases from 1 dB to 7 dB, all methods show degraded localization accuracy.

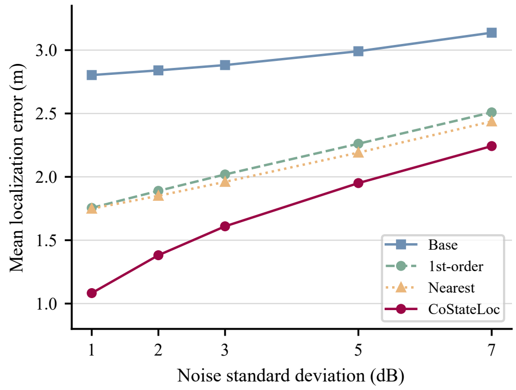

Fig. 14. Noise sensitivity in Layout A. The online RSS noise standard deviation is varied from 1 to 7 dB, and the mean localization error is reported for each method.

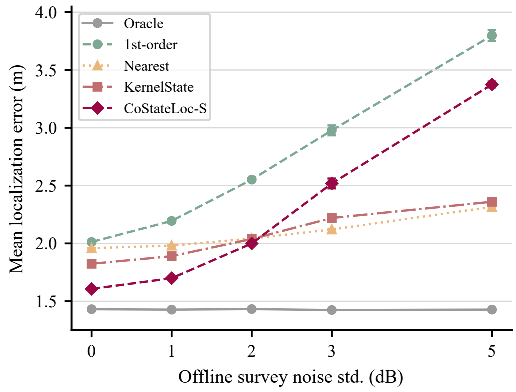

Fig. 15. Sensitivity to offline survey noise in Layout A. CoStateLoc-S denotes the noise-aware interaction-shrinkage variant in (15).

Nevertheless, CoStateLoc remains the best incomplete-survey method across the whole noise range. At 1 dB, CoStateLoc achieves a mean error of 1.08 m, while FirstOrder and NearestObs both give 1.75 m. At the default 3 dB setting, the corresponding errors are 1.61 m, 2.02 m, and 1.96 m, respectively. Even under the strongest tested noise level of 7 dB, CoStateLoc still outperforms FirstOrder, with 2.24 m compared with 2.51 m. The performance gap becomes smaller as the online measurements become noisier, because RSS observations are then less discriminative for WKNN matching. However, the consistent ordering of the methods indicates that the reconstructed radio map remains beneficial under moderate measurement noise.

Figure 15 reports the effect of noisy offline surveyed fingerprints. This is a stricter setting than the default experiment because the model components themselves are estimated from perturbed databases. With $\sigma_{\mathrm{off}} = 1$ dB, CoStateLoc-S obtains 1.70 m, compared with 1.89 m for KernelState and 2.20 m for FirstOrder. At $\sigma_{\mathrm{off}} = 2$ dB, CoStateLoc-S remains comparable to KernelState and NearestObs, with 2.00 m versus 2.04 m and 2.04 m, respectively. For stronger offline perturbations, however, KernelState and NearestObs become more robust than the interaction-based model. The unshrunk interaction model is especially sensitive because each interaction residual subtracts four noisy databases; its mean error reaches 3.41 m at 3 dB and 4.61 m at 5 dB. This result suggests that CoStateLoc should be used with averaged offline RSS fingerprints or with noise-aware interaction shrinkage when offline measurements are strongly noisy.

Figure 16 reports the AP-count sensitivity in the same layout. For each tested AP count, APs are regenerated with uniform spacing along the room length and alternating vertical offsets; the same AP set is then used by all methods. Since AP availability and AP discrimination are known to affect Wi-Fi fingerprint localization [14], [18], this experiment checks whether the observed gain depends on one particular AP configuration. Localization accuracy improves when more APs are available: CoStateLoc decreases from 1.72 m with four APs to 1.19 m with ten APs. FirstOrder follows the same trend but remains higher, decreasing from 2.10 m to 1.41 m. Therefore, the improvement is not tied to the default seven-AP setting; the pairwise reconstruction remains useful across sparse and denser AP deployments.

Figure 17 shows the sensitivity to state-label errors under the one-bit error model described in Sec. 6.1. As the state-label error rate increases from 0 to 30%, all state-aware methods degrade because the generated or selected radio map may correspond to a neighboring but incorrect environmental state. CoStateLoc increases from 1.607 m to 1.713 m, while FirstOrder increases from 2.017 m to 2.074 m and NearestObs from 1.960 m to 2.001 m. Therefore, the proposed reconstruction remains better than the incomplete-survey baselines under this mild state-identification error model. This experiment is an elementary perturbation test rather than a complete state-recognition study. Multiple simultaneous state errors or systematic state-classification bias would move the perceived state farther away from the true state in the binary state space and can cause larger localization degradation. Such cases require a dedicated environmental-state classifier, a confusion model, or a joint state-position estimator. The current result therefore confirms that CoStateLoc still requires a reasonably accurate state source in deployment.

The implementation time is reported only to document the experimental workflow on the platform in Tab. 3. It is not used as a hardware-independent efficiency claim. In Layout A, WKNN localization with a generated state-specific database takes 0.046 ms per query. Generating all 64 ray-traced state databases takes 87 s in the simulator; this is a one-time data-generation cost for evaluation and should not be interpreted as the real survey time saved by CoStateLoc. Once the surveyed databases are available, constructing the CoStateLoc model by computing $\boldsymbol{\delta}_h$ and $\mathbf{I}_{hq}$ takes less than 1 ms. The complexity analysis in Tab. 1 shows that the reconstruction cost scales linearly with M and N, and linearly with the number of retained components $H + K$. For the default $H = 6$, $K = 15$, $M = 80$, and $N = 7$ setting, storing the baseline, six main effects, and 15 pairwise terms requires $22MN = 12{,}320$ RSS values, which is about 96 kB if double-precision floating-point values are used. If all 42 unseen-state maps are cached, they require another $42MN = 23{,}520$ values, or about 184 kB. Therefore, the main practical cost addressed by this paper is the number of state-specific databases that must be surveyed, not the online computational burden.

Several limitations should be noted. First, the evaluation is based on a custom 2D ray-tracing simulator rather than real-world measurements. The simulator explicitly models distance-dependent loss, wall penetration, specular reflection, and coherent multipath combining, but it does not include diffraction, diffuse scattering, furniture and equipment, human blockage, device heterogeneity, AP power drift, 5/6 GHz operation, full 3D propagation, partially open doors, or attenuation from an opened door leaf near a wall. Therefore, the results represent a controlled mechanism study under the adopted propagation model, not direct proof of real-building accuracy. The comparison remains informative because all methods are tested under the same reproducible state space, AP layout, propagation model, and online-noise assumptions; however, real-world validation is necessary before deployment-level claims can be made. Second, the offline-noise experiment shows that directly computed pairwise interactions are sensitive when surveyed fingerprints are strongly noisy; practical deployment would require repeated offline sampling, averaging, or noise-aware interaction regularization. Third, the current evaluation assumes that the environmental state is available during online localization.

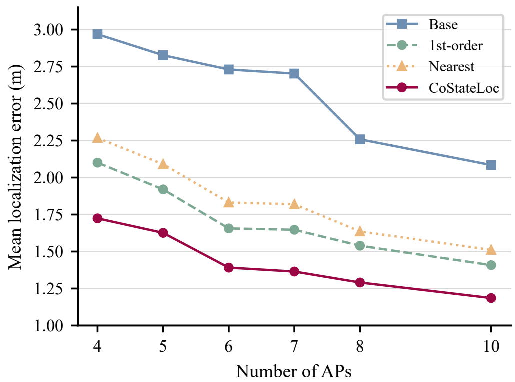

Fig. 16. AP-count sensitivity in Layout A. The number of APs is varied from 4 to 10 while all methods use the same AP configuration at each setting.

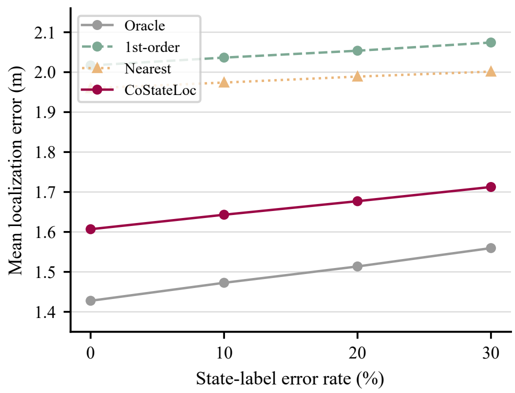

Fig. 17. Sensitivity to single-bit state-label errors in Layout A. The perceived environmental state is replaced by a one-bit-flipped state with probability p_s.

If the state is unknown, a state-estimation module must be introduced before applying CoStateLoc, for example by extending the state-identification idea used in multi-fingerprint localization [16]. Finally, all methods are evaluated with the same WKNN localizer; other localization back ends may change the absolute error values, although they would still require an unseen-state fingerprint database.

7. Conclusion

This paper addresses the scalability bottleneck left by the previous multi-fingerprint localization framework. While the earlier work established that variable spatial states should be represented by state-specific fingerprint databases, it required complete surveys over all environmental states [16]. CoStateLoc is proposed as a compositional state-conditioned fingerprint construction framework that constructs fingerprint databases for unseen environmental states from baseline, single-factor, and selected dual-factor surveys, reducing the required number of state-specific surveys from 2^H to $O(H^2)$.

Under the adopted 2D ray-tracing evaluation model, experiments with $H = 6$ doors across three geometrically different layouts show that CoStateLoc achieves 7.8–20.4% lower mean localization error than the first-order additive baseline while reducing the number of state-specific surveys by 65.6%. Its global RSS reconstruction RMSE is 36.1%, 51.0%, and 48.0% lower than FirstOrder in Layouts A, B, and C, respectively. With 22 surveyed states, its mean error remains within 0.18 m, 0.04 m, and 0.015 m of OracleFull, where OracleFull assumes all 64 state-specific fingerprint databases are available. CoStateLoc also outperforms the KernelState generator baseline in all three layouts. The state-order, online-noise, AP-count, state-label-error, offline-noise, and interaction-magnitude results show that the pairwise terms are most useful when the layout creates coupled propagation effects, but that they should be estimated from sufficiently averaged fingerprints or regularized under strong offline survey noise.

These conclusions are confined to the adopted controlled simulation setting and known-state evaluation protocol. They provide evidence for the proposed reconstruction mechanism rather than direct proof of accuracy in calibrated real buildings.

Future work will proceed in three directions. First, the framework will be validated with real-world measurements in an indoor deployment, so that device heterogeneity, human blockage, furniture, and temporal RSS drift can be tested directly. Second, the evaluation will be extended to multi-band Wi-Fi and independent 3D ray-tracing tools such as Sionna RT [41], including 5/6 GHz operation and more detailed propagation mechanisms. Third, CoStateLoc will be coupled with environmental-state sensing or joint state-position estimation, so that the known-state assumption used in this mechanism study can be relaxed in practical systems.

8. Data and Code Availability

The complete mathematical model of CoStateLoc is given in Secs. 3 and 4, and the ray-tracing data-generation model is specified in Sec. 5. To support reproducible research, the authors are willing to provide the simulation source code, layout configuration files, generated multi-state RSS datasets, and scripts used to reproduce the reported tables and figures upon reasonable request. Interested readers may contact the corresponding author for research-use access and reproduction assistance.

Acknowledgments

This work was supported by the Scientific Research Start-up Fund of Hubei Minzu University [grant number BS26019].

References

[1] LIU, H., DARABI, H., BANERJEE, P., et al. Survey of wireless indoor positioning techniques and systems. *IEEE Transactions on Systems, Man, and Cybernetics, Part C (Applications and Reviews)*, 2007, vol. 37, no. 6, p. 1067–1080. DOI: 10.1109/TSMCC.2007.905750

[2] ZAFARI, F., GKELIAS, A., LEUNG, K. K. A survey of indoor localization systems and technologies. *IEEE Communications Surveys & Tutorials*, 2019, vol. 21, no. 3, p. 2568–2599. DOI: 10.1109/COMST.2019.2911558

[3] BAHL, P., PADMANABHAN, V. N. RADAR: an in-building RF-based user location and tracking system. In *Proceedings of the IEEE International Conference on Computer Communications (INFOCOM)*. Tel Aviv (Israel), 2000, p. 775–784. DOI: 10.1109/INFCOM.2000.832252

[4] YOUSSEF, M., AGRAWALA, A. The Horus WLAN location determination system. In *Proceedings of the 3rd International Conference on Mobile Systems, Applications, and Services (MobiSys)*. Seattle (USA), 2005, p. 205–218. DOI: 10.1145/1067170.1067193

[5] HE, S., CHAN, S. H. G. Wi-Fi fingerprint-based indoor positioning: recent advances and comparisons. *IEEE Communications Surveys & Tutorials*, 2016, vol. 18, no. 1, p. 466–490. DOI: 10.1109/COMST.2015.2464084

[6] KHALAJMEHRABADI, A., GATSIS, N., AKOPIAN, D. Modern WLAN fingerprinting indoor positioning methods and deployment challenges. *IEEE Communications Surveys & Tutorials*, 2017, vol. 19, no. 3, p. 1974–2002. DOI: 10.1109/COMST.2017.2671454

[7] FANG, C., WANG, Y., ZHOU, M., et al. End-to-end human motion recognition with multidomain dual attention transformer fusion network and millimeter-wave radar. *IEEE Transactions on Consumer Electronics*, 2025, vol. 71, no. 2, p. 3252–3265. DOI: 10.1109/TCE.2025.3557084

[8] FANG, C., WANG, Y., ZHOU, M., et al. Cross-modal device-free radar sensing with information maximization enhancement and few-shot learning. *IEEE Transactions on Microwave Theory and Techniques*, 2026, vol. 74, no. 1, p. 1023–1036. DOI: 10.1109/TMTT.2025.3620482

[9] ROOS, T., MYLLYMAKI, P., TIRRI, H., et al. A probabilistic approach to WLAN user location estimation. *International Journal of Wireless Information Networks*, 2002, vol. 9, no. 3, p. 155–164. DOI: 10.1023/A:1016003126882

[10] HONKAVIRTA, V., PERAE, T., ALVAREZ, S., et al. A comparative survey of WLAN location fingerprinting methods. In *Proceedings of the 6th Workshop on Positioning, Navigation and Communication (WPNC)*. Hannover (Germany), 2009, p. 243–251. DOI: 10.1109/WPNC.2009.4907834

[11] SINGH, N., CHOE, S., PUNMIYA, R. Machine learning based indoor localization using Wi-Fi RSSI fingerprints: an overview. *IEEE Access*, 2021, vol. 9, p. 127150–127174. DOI: 10.1109/ACCESS.2021.3111083

[12] KAEMARUNGSI, K., KRISHNAMURTHY, P. Properties of indoor received signal strength for WLAN location fingerprinting. In *Proceedings of the First Annual International Conference on Mobile and Ubiquitous Systems: Networking and Services (MobiQuitous)*. Boston (USA), 2004, p. 14–23. DOI: 10.1109/MOBIQ.2004.1331706

[13] HE, S., HU, T., CHAN, S. H. G. Toward practical deployment of fingerprint-based indoor localization. *IEEE Pervasive Computing*, 2017, vol. 16, no. 2, p. 76–83. DOI: 10.1109/MPRV.2017.24

[14] WU, C., YANG, Z., ZHOU, Z., et al. Mitigating large errors in WiFi-based indoor localization for smartphones. *IEEE Transactions on Vehicular Technology*, 2017, vol. 66, no. 7, p. 6246–6257. DOI: 10.1109/TVT.2016.2630713

[15] HOU, C., XIE, Y., ZHANG, Z. FCLoc: A novel indoor Wi-Fi fingerprints localization approach to enhance robustness and positioning accuracy. *IEEE Sensors Journal*, 2023, vol. 23, no. 7, p. 7153–7167. DOI: 10.1109/JSEN.2022.3229476

[16] HOU, C., ZHANG, Z. Multi-fingerprints indoor localization for variable spatial environments: A naive Bayesian approach. *Sensors*, 2024, vol. 24, no. 18, p. 1–14. DOI: 10.3390/s24185940

[17] HOU, C., XIE, Y., ZHANG, Z. An improved convolutional neural network based indoor localization by using Jenks natural breaks algorithm. *China Communications*, 2022, vol. 19, no. 4, p. 291–301. DOI: 10.23919/JCC.2022.04.021

[18] KUSHKI, A., PLATANIOTIS, K. N., VENETSANOPOULOS, A. N. Kernel-based positioning in wireless local area networks. *IEEE Transactions on Mobile Computing*, 2007, vol. 6, no. 6, p. 689–705. DOI: 10.1109/TMC.2007.1017

[19] WANG, X., GAO, L., MAO, S. CSI phase fingerprinting for indoor localization with a deep learning approach. *IEEE Internet of Things Journal*, 2016, vol. 3, no. 6, p. 1113–1123. DOI: 10.1109/JIOT.2016.2558659

[20] HOSSAIN, A. K. M. M., SOH, W. S. A survey of calibration-free indoor positioning systems. *Computer Communications*, 2015, vol. 66, p. 1–13. DOI: 10.1016/j.comcom.2015.03.001

[21] CHINTALAPUDI, K., IYER, A. P., PADMANABHAN, V. N. Indoor localization without the pain. In *Proceedings of the 16th Annual International Conference on Mobile Computing and Networking (MobiCom)*. Chicago (USA), 2010, p. 173–184. DOI: 10.1145/1859995.1860016

[22] RAI, A., CHINTALAPUDI, K. K., PADMANABHAN, V. N., et al. Zee: zero-effort crowdsourcing for indoor localization. In *Proceedings of the 18th Annual International Conference on Mobile Computing and Networking (MobiCom)*. Istanbul (Turkey), 2012, p. 293–304. DOI: 10.1145/2348543.2348580

[23] JUNG, S. H., HAN, D. Automated construction and maintenance of Wi-Fi radio maps for crowdsourcing-based indoor positioning systems. *IEEE Access*, 2017, vol. 6, p. 1764–1777. DOI: 10.1109/ACCESS.2017.2780243

[24] HE, S., LIN, W., CHAN, S. H. G. Indoor localization and automatic fingerprint update with altered AP signals. *IEEE Transactions on Mobile Computing*, 2017, vol. 16, no. 7, p. 1897–1910. DOI: 10.1109/TMC.2016.2608946

[25] SUN, Y., HE, Y., MENG, W., et al. Voronoi diagram and crowdsourcing-based radio map interpolation for GRNN fingerprinting localization using WLAN. *Sensors*, 2018, vol. 18, no. 10, p. 1–17. DOI: 10.3390/s18103579

[26] CANDES, E. J., RECHT, B. Exact matrix completion via convex optimization. *Foundations of Computational Mathematics*, 2009, vol. 9, no. 6, p. 717–772. DOI: 10.1007/s10208-009-9045-5

[27] KOLDA, T. G., BADER, B. W. Tensor decompositions and applications. *SIAM Review*, 2009, vol. 51, no. 3, p. 455–500. DOI: 10.1137/07070111X

[28] JIANG, W., NIU, Q., HE, S., et al. Adaptive radio map reconstruction via adversarial wireless fingerprint learning. *Neural Computing and Applications*, 2023, vol. 35, no. 25, p. 18585–18602. DOI: 10.1007/s00521-023-08684-w

[29] LI, X., ZHANG, S., LI, H., et al. RadioGAT: A joint model-based and data-driven framework for multi-band radiomap reconstruction via graph attention networks. *IEEE Transactions on Wireless Communications*, 2024, vol. 23, no. 11, p. 17777–17792. DOI: 10.1109/TWC.2024.3457157

[30] CHEN, Y., DONG, C., NIU, K. Radio map estimation for indoor localization using conditional generative adversarial network. In *Proceedings of the 2024 10th International Conference on Communication and Information Processing*. Lingshui (China), 2024, p. 353–358. DOI: 10.1145/3708657.3708714

[31] LUO, X., LI, Z., PENG, Z., et al. RM-Gen: Conditional diffusion model-based radio map generation for wireless networks. In *Proceedings of the 2024 IFIP Networking Conference (IFIP Networking)*. Thessaloniki (Greece), 2024, p. 543–548. DOI: 10.23919/IFIPNetworking62109.2024.10619829

[32] WANG, S., ZHANG, S., MA, J., et al. Graph-neural-network-based WiFi indoor localization system with access point selection. *IEEE Internet of Things Journal*, 2024, vol. 11, no. 20, p. 33550–33564. DOI: 10.1109/JIOT.2024.3430087

[33] PAN, S. J., YANG, Q. A survey on transfer learning. *IEEE Transactions on Knowledge and Data Engineering*, 2010, vol. 22, no. 10, p. 1345–1359. DOI: 10.1109/TKDE.2009.191

[34] WANG, J., FU, Y., FENG, H., et al. Transfer learning for indoor localization algorithm based on deep domain adaptation. *Sensors*, 2023, vol. 23, no. 23, p. 1–20. DOI: 10.3390/s23239334

[35] FRIIS, H. T. A note on a simple transmission formula. *Proceedings of the IRE*, 1946, vol. 34, no. 5, p. 254–256. DOI: 10.1109/JRPROC.1946.234568

[36] RAPPAPORT, T. S. *Wireless Communications: Principles and Practice*. 2nd ed. Upper Saddle River (USA): Prentice Hall, 2002. ISBN: 0130422320

[37] SEIDEL, S. Y., RAPPAPORT, T. S. 914 MHz path loss prediction models for indoor wireless communications in multifloored buildings. *IEEE Transactions on Antennas and Propagation*, 1992, vol. 40, no. 2, p. 207–217. DOI: 10.1109/8.127405

[38] GOLDSMITH, A. *Wireless Communications*. Cambridge (United Kingdom): Cambridge University Press, 2005. ISBN: 978-0-521-83716-3

[39] ITU-R. Recommendation ITU-R P.1238-13 (09/2025): Propagation Data and Prediction Methods for the Planning of Indoor Radiocommunication Systems and Radio Local Area Networks in the Frequency Range From 300 MHz to 450 GHz *International Telecommunication Union*, Geneva, 2025.

[40] LAURENSON, D. I., MCLAUGHLIN, S., SHEIKH, A. A ray tracing approach to channel modelling for the indoor environment. In *Proceedings of the IEEE 43rd Vehicular Technology Conference (VTC)*. Secaucus (USA), 1993, p. 246–249. DOI: 10.1109/VETEC.1993.507107

[41] HOYDIS, J., AIT AOUDIA, F., CAMMERER, S., et al. Sionna RT: Differentiable ray tracing for radio propagation modeling. arXiv:2303.11103, 2023, p. 1–12. DOI: 10.48550/arXiv.2303.11103

[42] HOU, C., XIE, Y., ZHANG, Z. Multi-fingerprint localization in complex dynamic indoor environments based on Gaussian mixture model clustering. In *Proceedings of the IEEE Global Communications Conference (GLOBECOM)*. Taipei (Taiwan), 2025, p. 4736–4741. DOI: 10.1109/GLOBECOM59602.2025.11431706

[43] MONTGOMERY, D. C. *Design and Analysis of Experiments*. 10th ed. Hoboken (USA): Wiley, 2020. ISBN: 978-1119634256

[44] COVER, T., HART, P. Nearest neighbor pattern classification. *IEEE Transactions on Information Theory*, 1967, vol. 13, no. 1, p. 21–27. DOI: 10.1109/TIT.1967.1053964

[45] SAUNDERS, C., GAMMERMAN, A., VOVK, V. Ridge regression learning algorithm in dual variables. In *Proceedings of the 15th International Conference on Machine Learning (ICML)*. Madison (USA), 1998, p. 515–521.

About the Authors ...

Chengjie HOU (corresponding author) received the M.Sc. degree in Electronic and Computer Engineering from the University of Birmingham, United Kingdom, in 2018, and the Ph.D. degree in Information and Communication Engineering from Chongqing University of Posts and Telecommunications, China, in 2025. He is currently a lecturer with the College of Intelligent Systems Science and Engineering, Hubei Minzu University, Enshi, China. His research interests include fingerprint localization, radio map construction, and intelligent sensing.

Xianbo SUN received the M.Eng. degree in Control Theory and Control Engineering and the Ph.D. degree in Traffic Information Engineering and Control from Wuhan University of Technology, China, in 2008 and 2019, respectively. He is currently a professor and master's supervisor with the College of Intelligent Systems Science and Engineering, Hubei Minzu University, Enshi, China. His research interests include control theory and control engineering, industrial automation, and the Internet of Things.

Yong HUANG received the M.Eng. degree in Instrument Science and Technology from Chongqing University, China, in 2008, and the Ph.D. degree in Electronic Science and Technology from Huazhong University of Science and Technology, China, in 2017. He is currently a professor and master's supervisor with the College of Intelligent Systems Science and Engineering, Hubei Minzu University, Enshi, China. His research interests include electronic system design and simulation, wireless sensor networks, intelligent control, and high-reliability MOSFET devices.

Qinghua ZHU received the M.Eng. degree in Traffic Information Engineering and Control and the Ph.D. degree in Vehicle Operation Engineering from Shanghai Maritime University, China, in 2022 and 2025, respectively. He is currently a faculty member with the College of Intelligent Systems Science and Engineering, Hubei Minzu University, Enshi, China. His research interests include transportation engineering, safety engineering, and intelligent ships.

Jinqiao YI received the M.Sc. degree in Applied Mathematics from Northwest Normal University, China, in 2006, and the Ph.D. degree in Microelectronics and Solid-State Electronics from Huazhong University of Science and Technology, China, in 2015. He is currently a professor and master's supervisor with Hubei Minzu University, Enshi, China. His research interests include optoelectronic materials and applications, Internet of Things technology and intelligent systems, and power Internet of Things technology.

Tao HU received the M.Eng. degree in Software Engineering from Peking University, China, in 2009, and the Ph.D. degree in Computer Technology from Wuhan University, China, in 2020. He is currently a professor with Hubei Minzu University, Enshi, China. His research interests include computer vision, artificial intelligence, and video big data processing.

Lin GAO received the M.Eng. degree in Control Engineering from Wuhan University of Technology, China, in 2007, and the Ph.D. degree in Mechatronic Engineering from Sichuan University, China, in 2020. He is currently an associate professor and master's supervisor with the College of Intelligent Systems Science and Engineering, Hubei Minzu University, Enshi, China. His research interests include artificial intelligence, computer vision, and embedded systems.

Li ZHU received the M.Eng. degree in Communication and Information Systems from China University of Geosciences, Wuhan, China, in 2009. She is currently an associate professor and master's supervisor with the College of Intelligent Systems Science and Engineering, Hubei Minzu University, Enshi, China. Her research interests include intelligent sensing for the Internet of Things, wireless sensor networks, and fault prediction and diagnosis of electrical equipment.